Journal of Glaciology

Article

Cite this article: Fowler JR, Iverson NR (2022). A permeameter for temperate ice: first results on permeability sensitivity to grain size. *Journal of Glaciology* 1–11. https://doi.org/10.1017/jog.2021.136

Received: 29 July 2021
Revised: 10 December 2021
Accepted: 13 December 2021

Key words:
Glacier flow; glacier hydrology; glaciological instruments and methods; ice physics; ice streams

Author for correspondence:
Neal R. Iverson,
E-mail: niverson@iastate.edu

cambridge.org/jog

A permeameter for temperate ice: first results on permeability sensitivity to grain size

Jacob R. Fowler and Neal R. Iverson

Department of Geological and Atmospheric Sciences, Iowa State University, Ames, Iowa 50011, USA

Abstract

Results of ice-stream models that treat temperate ice deformation as a two-phase flow are sensitive to the ice permeability. We have constructed and begun using a custom, falling-head permeameter for measuring the permeability of temperate, polycrystalline ice. Chilled water is passed through an ice disk that is kept at the pressure-melting temperature while the rate of head decrease indicates the permeability. Fluorescein dye in the water allows water-vein geometry to be studied using fluorescence microscopy. Water flow over durations of seconds to hours is Darcian, and for grain diameter d increasing from 1.7 to 8.9 mm, average permeability decreases from 2×10^{-12} to 4×10^{-15} m^2. In tests with dye on fine ($d = 2$ mm) and coarse ($d = 7$ mm) ice, average area-weighted vein radii are nearly equal, 41 and 34 μm, respectively. These average radii, if included in a theory slightly modified from Nye and Frank (1973), yield permeability values within a factor of 2.0 of best-fit values based on regression of the data. Permeability values depend on $d^{-3.4}$, rather than d^{-2} as predicted by models if vein radii are considered independent of d. In future experiments, the dependence of permeability on liquid water content will be measured.

1. Introduction

Flow of marine-terminating ice streams accounts for most of the mass lost from the Antarctic Ice Sheet (Rignot and others, 2019) and about half of the mass lost from the Greenland Ice Sheet (IMBIE Team, 2020). Fast flow of these glaciers is regulated fundamentally by water. Water at the bed enables low effective stress and basal slip, accompanied by low basal drag (e.g. Kamb, 2001). In addition, shear heating in ice-stream margins dissipates sufficient heat to overcome the effects of cold-ice advection from the glacier surface and from adjacent slow-moving ice to cause many margins to be temperate at depth (Meyer and Minchew, 2018). Interstitial water in the temperate ice reduces its effective viscosity (Duval, 1977; Adams and others, 2021), affecting the shearing resistance, velocity distribution and strain heating of shear margins (Haseloff and others, 2019). Water, through its substantial latent heat, also influences the energy balance that dictates ice temperature (Schoof and Hewitt, 2016) and its feedback on ice effective viscosity (e.g. Minchew and others, 2018). Moreover, water production in shear margins controls the supply of water to the underlying bed. This basal water helps control the lateral distribution of basal effective stress and drag (Suckale and others, 2014; Perol and Rice, 2015; Meyer and others, 2018; Haseloff and others, 2019). Ice softening by interstitial water that localizes strain in ice-stream shear margins (Haseloff and others, 2019) also creates troughs at their surfaces that accelerate ocean-driven break-up of ice shelves (Alley and others, 2019).

Including these kinds of dependencies in models of ice streams is a major goal of the glaciological community (Suckale and others, 2014; Kyrke-Smith and others, 2014, 2015; Haseloff and others, 2015; Perol and Rice, 2015; Perol and others, 2015; Platt and others, 2016; Meyer and others, 2018; Haseloff and others, 2019; Hunter and others, 2021). This goal cannot be achieved without estimating distributions of ice temperature and water content and the position of the boundary between cold and temperate ice. Although the development of the necessary theory has been ongoing for some time, with various assumptions regarding water transport in temperate ice (e.g. Hutter, 1982; Greve, 1997; Aschwanden and Blatter, 2009; Aschwanden and others, 2012), the recent formulations of Schoof and Hewitt (2016) and Hewitt and Schoof (2017), which build on Fowler (1984), highlight the importance of interstitial water flow driven by gravity and pressure gradients, a point also emphasized by Nye (1991a). To relate the volume flux of water to gravity and pressure gradients, Darcian flow of water through ice is assumed, and permeability is considered to have a power-law dependence on water content (= porosity, if ice is water-saturated). Ice is treated as compressible, somewhat analogous to water-saturated poroelastic media, but with viscous deformation of ice controlling compaction through creep closure of pores and associated water flow.

Haseloff and others (2019), in the most explicit effort to date to include the softening effect of water in an ice-stream model, made these assumptions to treat temperate parts of margins as a two-phase flow, with gravity-driven water transport through ice at the grain scale. Their study emphasized how the softening effect of water on ice can localize strain in shear margins, focus heat dissipation and increase meltwater production and delivery to the bed, where this water affects basal slip.

In the modeling of Haseloff and others (2019), the poorly known permeability of glacier ice was the largest source of uncertainty. Permeability coefficients ranging through four orders of magnitude were deemed possible. At the high end of this range, effectively all meltwater

produced by shear heating drained away, leading to a negligibly small meltwater content in most of the temperate part of the shear zone. In contrast, at the lowest permeability value thought to be possible, drainage was inhibited sufficiently to result in a water content of ∼8%, well above the range over which the effect of water on ice softening is known (Duval, 1977; Adams and others, 2021) and above values observed at the grain scale in glacier ice (<3%). Previous models of ice-stream shear margins that routed meltwater to the bed (but did not include the softening effect of water from shear heating) would have also benefited from reliable permeability values for temperate ice (Suckale and others, 2014; Meyer and others, 2018).

Despite the uncertainty of permeability values, the ability of water to flow through temperate ice at the grain scale is well established. Microscopic observations of temperate ice (Nye and Mae, 1972; Nye and Frank, 1973; Raymond and Harrison, 1975; Mader, 1992) demonstrate that water resides in veins where three grains meet, where veins intersect to form nodes, and in lenses along grain boundaries oriented optimally with respect to principal stresses in the ice. Together these water bodies at grain boundaries constitute an interconnected system of channels (Nye, 1989). Various theoretical efforts have been made to estimate or place limits on the permeability of temperate ice (Nye and Frank, 1973; Raymond and Harrison, 1975; Lliboutry, 1996). Estimations and measurements of the permeability of rocks with small melt fractions similar to those of temperate ice suggest power-law dependencies on grain size and porosity (e.g. McKenzie, 1984; Miller and others, 2014). In glacier models, the dependence on grain size is left implicit, whereas the power-law dependence on porosity (exponent of ∼2) is adopted explicitly (e.g. Haseloff and others, 2019; Schoof and Hewitt, 2016).

Given the importance of temperate ice, water production and water routing in glacier flow and the widespread acknowledgement that temperate ice is indeed permeable, a reasonable expectation might be that the permeability of glacier ice and its dependence on grain size and water content would have a sound empirical basis. Surprisingly, however, no experiments, excluding one that yielded a permeability value most relevant to unsaturated flow (Jordan and Stark, 2001), have been conducted to measure the permeability of temperate ice or even to demonstrate that water flow through ice obeys a Darcian rule. Thus, theoretical models of ice permeability, based on the geometry of idealized water-vein networks, cannot be tested, and ice-stream models that rely on estimating ice permeability yield results that are illustrative but not prognostic.

Therefore, we have designed, constructed and begun to use a laboratory permeameter for measuring the flow resistance of water through temperate, polycrystalline ice. The goal here is to describe the device in detail and present data from initial experiments that test the important assumptions of Darcian flow and the power-law dependence of ice permeability on grain size. Although experiments with the new device fall short of simulating steady, long-term, grain-scale flow of water through glacier ice, they provide measured values of permeability formerly absent for guiding two-phase models of glacier flow. Moreover, these experiments provide a means of testing, for the first time, simplified models of ice permeability based on Poiseuille flow of water through geometrically idealized vein networks.

2. Background and objectives

Darcy's law for steady, laminar flow of water through porous media is

$$\mathbf{q} = \frac{-k\rho g}{\mu}\nabla h, \tag{1}$$

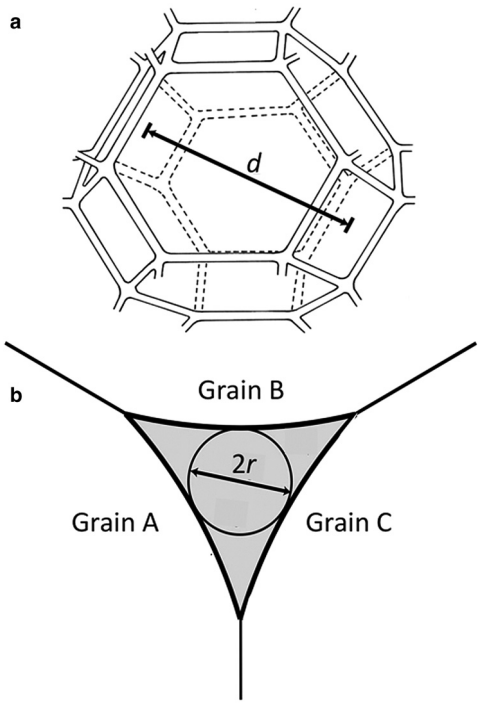

Fig. 1. (a) Network of melt veins (like that considered by Frank (1968)) approximated by truncated semiregular octahedra (modified from Dani and others, 2012). (b) Cross-section of a water vein at a three-grain intersection, with vein radius, r, describing the size of an equilateral triangle used to model Poiseuille flow through veins.

where $\mathbf{q}$ is the specific discharge vector, ρ is water density, g is the gravitational acceleration, μ is the water viscosity, and h is the hydraulic head. Theories for the permeability of rock with small melt fractions idealize grain shape and size distribution, the associated network of melt-filled veins at grain boundaries, and vein cross-sectional areas (Frank, 1968; McKenzie, 1984; Zhu and Hirth, 2003). Consideration of Poiseuille flow through melt-filled vein networks bounding grains under a head gradient $\mathrm{d}h/\mathrm{d}x$ yields the specific discharge:

$$q = -B\frac{r^4}{d^2}\frac{\rho g}{\mu}\frac{\mathrm{d}h}{\mathrm{d}x} \tag{2}$$

with

$$k = B\frac{r^4}{d^2}, \tag{3}$$

where d is the grain diameter, r is the radii of individual veins, and B is a dimensionless constant that depends on the vein cross-sectional shape and vein network geometry (Fig. 1) (e.g. Frank, 1968).

For grain shapes idealized as truncated octahedra, as in most models of ice vein networks (Nye and Frank, 1973; Price, 2000; Mader and others, 2006; Dani and others, 2012), and Poiseuille flow through vein cross-sections idealized as equilateral triangles (Lekner, 2007), $B = 1.33$. This value is ∼20% larger than the value for circular cross-sections (Nye and Frank, 1973), despite a slightly smaller mean discharge per unit area in triangular sections (Lekner, 2007), because triangular sections have larger areas than circular sections for a given vein radius as defined in Figure 1. Defining ϕ as the fractional melt content, $\phi \propto (r/d)^2$. Thus, if ϕ is a constant that does not vary with grain diameter, $r \propto \phi^{1/2}d$, so that Eqn (3) yields a power law for the permeability

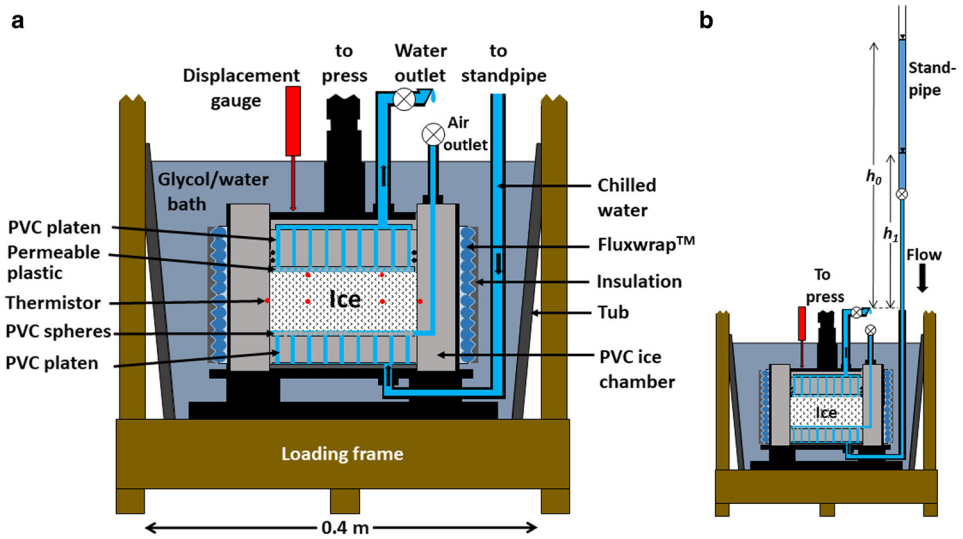

Fig. 2. Schematic cross-section of the permeameter. (a) Ice chamber and surrounding bath. Red dots are thermistor locations. (b) Ice chamber with standpipe (not to scale). The device resides in a walk-in freezer. The external hydraulic pump/press and heating/cooling circulator are not shown (see colors in on-line version).

of rocks with small melt fractions:

$$k = C\phi^2 d^2, \tag{4}$$

where C depends on an assumed vein and vein network geometry (e.g. Frank, 1968; McKenzie, 1984; Miller and others, 2014). This equation is thought to be appropriate for isotropic melt-bearing rocks with uniform grain size and shape (Miller and others, 2014).

Herein, with results from an initial set of experiments, we test the usual assumption that water flow through ice is Darcian and the hypothesis that, if vein size is independent of grain size, permeability varies with the inverse square of grain size (Eqn 3). The value of B and the inverse-square dependence on grain size are necessarily based on idealizations: that veins are straight, continuous and all contribute to the movement of water along grain boundaries. In contrast, veins in polycrystalline ice at atmospheric pressure observed in experiments are commonly discontinuous and irregular in shape (Mader, 1992). Another complication is air bubbles that are thought to plug some veins (Lliboutry, 1971, 1996; Raymond and Harrison, 1975). We have only just begun the measurements of ice water content, and the system for measuring it was not complete when the initial data presented herein were collected, so we defer data to test Eqn (4) through measurement of k and ϕ to a subsequent paper.

3. Device

The new device allows the water-saturated permeability of ice to be measured at the pressure-melting temperature (PMT). The principle used is that of a falling-head permeameter (Fig. 2), as applied commonly to fine-grained soils (e.g. silt; Lambe and Whitman, 1969). In the new device, an initial hydraulic head is applied to a confined disk of ice, 140 mm diameter and up to 70 mm thick (Fig. 2a), and the decrease in head with time is measured to determine permeability. More specifically, the chilled-water discharge associated with the rate of head decrease in a standpipe of known volume is equated with the Darcian discharge of water through the thickness of the ice disk. Integrating this equality with respect to time yields the intrinsic permeability, k:

$$k = \frac{aH\mu}{A\rho g t}\ln\left(\frac{h_0}{h_1}\right), \tag{5}$$

where a and A are the cross-sectional areas of the standpipe and ice disk, respectively, H is the thickness of the disk, h_0 is the initial hydraulic head, and h_1 is head after some time, t, has elapsed (Todd, 1961) (Fig. 2b).

Although Eqn (5) is a standard formulation (e.g. Freeze and Cherry, 1979), the new device needed to meet a number of special criteria for this application: ice samples kept at the pressure-melting temperature without melting them prohibitively fast; ice samples large enough in diameter to allow experiments with coarse-grained ice; cylindrical ice specimens to allow easy study of ice cored from glaciers; ice subjected to a confining pressure; water not allowed to move preferentially along the edges of the ice specimen; hydraulic gradients across ice specimens that are minimized; and a precise means of measuring the liquid water content of the ice. Most importantly, the method for measuring permeability needed to be simple and thus likely to succeed, which led us to the falling-head technique. A constant-head experiment (e.g. Freeze and Cherry, 1979), with the water discharge through the ice specimen measured, would also be possible with minimal changes to the device but would carry with it the problem of including meltwater from the disk in the measured water discharge, a potential source of uncertainty for low-permeability ice.

3.1 Ice chamber

The ice disk is confined in a cylindrical chamber that allows water to flow upward through the disk (Fig. 2). The cross-sectional area through which water flows is a factor of ~50–15 000 larger than areas of individual ice crystals 1–20 mm in diameter (~1–320 mm^2). PVC plastic, 38 mm thick and a thermal insulator, confines the ice disk on its sides, and this plastic also constitutes the platens that push vertically on the disk. These platens contain vertical holes that convey water to and from thin (6 mm) permeable plastic sheets at their surfaces. The sheets can consist of either permeable plastic or a layer of plastic spheres one sphere-diameter thick. These sheets ensure that water is conveyed uniformly to and from the disk faces over their full areas. A conduit from the perimeter of the lower sheet extends upward through the PVC walls to allow air to escape that would otherwise impede water flow. To strengthen the plastic of the ice chamber, it is surrounded on its sides by a thin stainless-steel wall.

3.2 Ice temperature control

The system for controlling temperature is like that used to successfully keep ice at the pressure-melting temperature in ring-shear experiments (Iverson and Petersen, 2011; Zoet and Iverson, 2020; Thompson and others, 2020). The permeameter resides in a cold room kept at 1.0 ± 0.5°C, which alone is inadequate for temperature control. Thus, the ice chamber is submerged in a bath consisting of a water/ethylene glycol mixture (Fig. 2a). The bath is contained in a plastic tub that is plumbed to an external heating/cooling circulator, which pumps the fluid into and out of the bath and regulates the temperature to ~0.01°C higher than the PMT of the ice. Together with the thick insulating walls of the ice chamber, this temperature difference minimizes the heat flux to the ice disk. Melting of ice disks is thus minimized, so head decreases can, if necessary, be measured for up to ~3 weeks before the ice disk becomes too thin. This allows permeability values as low as $\sim 10^{-18}\,\mathrm{m}^2$ to be measured, comparable to the lowest values expected for ice (Raymond and Harrison, 1975).

3.3 Pressure control

A downward stress of 250–1500 kPa can be exerted on the ice by the upper platen, which is driven by an air-powered, hydraulic pump. As melting occurs at the boundaries of the ice specimen and water drains, the upper platen moves downward, keeping the downward stress on the ice steady and generating lateral stress in the ice that presses it against the walls of the ice chamber. This lateral stress, which greatly exceeds the pressure head applied to the base of the ice disk, prevents water introduced to the base of the ice disk from flowing in the water film along the disk's edges. Rather, only meltwater produced by melting at the disk edges flows there, toward the top and bottom of the disk. Downward motion of the upper platen, which mainly reflects melting of the ice disk, is measured to the nearest 0.01 mm with an LVDT or dial gauge. The resultant thinning rate of the ice disk can be kept as small as $\sim 1.5\,\mathrm{mm\,d}^{-1}$.

3.4 Head and water flow

The device's graduated standpipe (Fig. 2b), with an inside diameter of 11 mm, can extend up to $h_0 = 2.0$ m. Water from it flows first downward into the bath and then upward into the base of the sample chamber. Importantly, all water used in the experiment is first chilled to 0°C in an ice-water bath, to inhibit advection of heat in water to the ice. After passing through the ice disk, water flows upward through the upper platen and then through tubing to an external drain kept at constant elevation. Once water is steadily flowing from this drain, a valve on its end (Fig. 2a) is closed, and the head is raised to an initial value, h_0, by adding water to the standpipe (Fig. 2b). To start an experiment, this valve is opened, and head is allowed to fall to a lower value, h_1, while the falling head in the standpipe is measured.

The success of this process depends on interstitial water pressure within the ice disk being smaller than the pressure head applied to the base of the ice disk. If this condition is not met, the introduced water will not flow through the disk. Although the design of the ice chamber minimizes heat flow to the disk and its thinning by melting at its boundaries, heat is nevertheless conducted into the ice disk from its perimeter. This heat flow causes melting within the ice disk and results from the process that 'rots' temperate ice, as described by Nye (1991b). Owing to the curvature of water-vein walls, their PMT is slightly less than the boundaries of the ice specimen, causing inward heat flow that melts ice at vein walls. In ice at atmospheric pressure, this process causes veins and water films to grow, so that assemblies of ice crystals eventually disaggregate (i.e. rot). The ice disks here are under a confining pressure, so internal melting and associated vein growth should be accompanied by vein pressurization that increases with time. This hypothesis explains an observation from initial experiments with the permeameter: if ice was kept under a confining pressure and at the PMT for more than several days, water flow through the ice disk did not occur, and ice permeability could not be measured. Thus, there is a limited time window for successful experiments; they must be conducted after the full ice disk is at the PMT but before internal melting has increased vein water pressure sufficiently.

3.5 Measurement of water content

To measure the liquid water content of ice, the device is configured to use the calorimetric method of our ice-deformation experiments (Adams and others, 2021, see also Duval, 1976). The lateral edges of the ice disk can be abruptly chilled to below the PMT, and the speed of the resultant freezing front that moves radially inward can be tracked with thermistors in the ice. Fitting the solution to the associated Stefan problem to arrival times of the freezing front at thermistors provides a high-resolution measure of water content, owing to the high latent heat of fusion of water that markedly slows the freezing front. A flexible jacket (North Slope Chillers Fluxwrap™), wrapped around the vertical walls of the ice chamber, is used to cool the ice-disk walls immediately after measuring the ice permeability (Fig. 2a). The jacket contains coiled fluid conduits that carry a chilled glycol/water mixture, pumped and temperature-controlled by an external circulator. Thermistors at the inner walls of the ice chamber provide the time-dependent, temperature boundary condition for the Stefan problem (Asaithambi, 1988), and two thermistors in the ice disk track the freezing front. Thick PVC bounding the ice disk at its top and bottom helps ensure that heat flow paths are dominantly horizontal. Nevertheless, thermistors at the top of the ice disk detect whether the freezing front advances non-uniformly; if so, this effect can be accounted for by adding the vertical dimension to the Stefan problem and its finite-difference solution.

As alternative means of measuring water content in ice, we have explored over the last 3 years both capacitance-based techniques (Kizito and others, 2008) and time-domain reflectometry (TDR) (e.g. Robinson and others, 2003). However, neither of these techniques, which are applied routinely to soils, provides resolution at low water contents (<5%) comparable to that provided by the calorimetric method. Application of TDR to frozen soils is consistent with this conclusion (Zhou and others, 2014), as is application of TDR to ice cores (West and others, 2007).

4. Procedure

Isotropic polycrystalline ice disks are made following the sample preparation method described by Duval and Le Gac (1980). Sieved snow grains, made from de-ionized water, are packed into a cylindrical mold with thick insulating walls. A vacuum is applied to the snow disk, and at its base chilled, deionized, de-aired water is introduced so that water flows upward into pore spaces. Placing a thick, chilled aluminum plate at the base of the disk freezes the water-saturated snow from the bottom up, resulting in ice that is free of large air bubbles but still contains sparse, smaller bubbles (<300 μm). Ice crystals have no significant preferred orientation, and the range of sizes is controlled by the size range of the sieved snow particles.

An ice disk is added to the permeameter, and its edges are sealed by freezing chilled deionized water in the submillimeter-wide gap

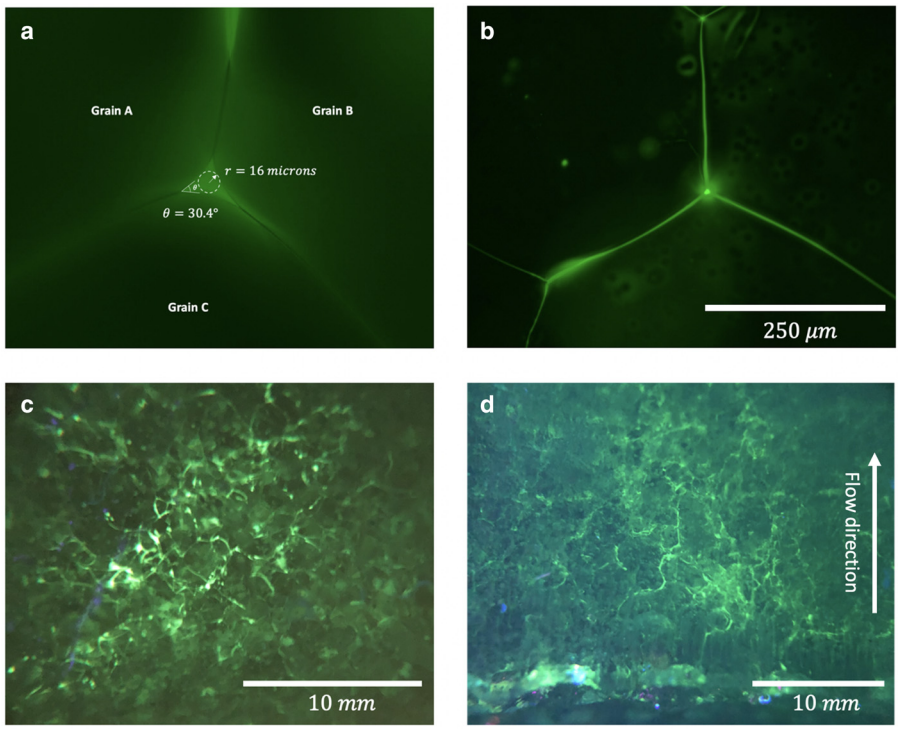

Fig. 3. (a) Former water-filled vein at a three-grain intersection imaged using through-flowing water that contained fluorescein dye. Despite the need to freeze the interstitial water to make thin sections, the dye preserves the cross-sectional form of veins, allowing measurements of vein radius, r, and dihedral angle, θ. (b) Former water at three-grain intersections and grain boundaries as imaged in thin section by the dye. (c) Water-filled vein network in a fine-grained ice specimen still at its melting temperature immediately after a permeability experiment. In parts a–c, water flow was approximately normal to the plane of the photograph. (d) Flow pathways viewed in a plane parallel to water flow in a fine-grained ice specimen at its melting temperature (see colors in on-line version).

that divides the disk from the walls of the ice chamber. A confining pressure is applied to the disk, and it is brought to the PMT by increasing the temperature of the glycol/water bath to ~0.01°C above the expected PMT. Downward movement of the upper platen indicates the initiation of melting, but permeability measurements are delayed for at least a day to ensure that production of intercrystalline water extends to the center of the ice disk. Temperatures recorded by thermistors indicate when the PMT is reached.

Permeability tests are then conducted in succession over several ranges of head spanning 0.01–2 m. To measure ice permeability, chilled water, decanted from freezing slush, is first added to the device's standpipe. This through-flowing water introduced to the ice for permeability tests sometimes contains fluorescein dye at low concentration (10 mg L^{-1}). Fluorescein is particularly well suited as a tracer owing to its detectability at very low concentrations, and its stability and inertness in the presence of ice surfaces (Eicken and others, 2002). Measurements with a high-precision thermistor (±0.001°C) indicate that the effect of this dye on the PMT is negligible. Head is recorded either by videotaping the falling water elevation in the standpipe or by measuring the elevation directly to the nearest millimeter if head decreases sufficiently slowly. Head decreases are executed at initial head values increasing from 0.5 to 2.0 m, and sometimes a second series of head tests is performed thereafter at the same 0.5–2.0 m head values. The latter value corresponds to a maximum hydraulic gradient of ~35. After the falling-head tests, pressure is removed from the ice disk, its edges are warmed, and the disk is extracted from the ice chamber.

Fluorescence, as revealed in thin sections and larger sections of ice disks still at the melting temperature, yields clear images of the former water-vein system (Fig. 3). The thin-section observations provide water-vein cross-sectional geometries (Fig. 3a, b) and allow measurement of vein radii. Dye also highlights flow pathways (Fig. 3c, d). Preservation of the fine-scale details of vein cross-sections (Fig. 3a), such as the dihedral angle (32 ± 3°, Nye and Mae, 1972) and the convexity of vein boundaries, argues for dyed zones accurately reflecting vein size and shape.

Grain geometry is also measured in thin sections following Fitzpatrick (2013). Equivalent diameter distributions of the ice grains are measured by photographing thin sections on a Rigsby stage and separating individual grains along one-pixel boundaries to analyze grain areas. Grain sizes are corrected to account for measurement bias in a plane following Durand (2004). The irregularity of grain boundaries, called herein the tortuosity, is determined by measuring the length of an ice-grain perimeter and dividing by the circumference of a circle computed from the grain's area.

Table 1. Grain diameter, permeability and vein size for the seven ice specimens of Figure 7

Ice specimen	Grain diameter, mm	Permeability, m^2	Mean vein size, μm
1	1.7 ± 0.4	$2 \pm 1.4 \times 10^{-12}$	35 ± 20
2	2.6 ± 1.2	$7 \pm 4.2 \times 10^{-13}$	–
3	3.4 ± 1.0	$5 \pm 1.5 \times 10^{-13}$	–
4	5.2 ± 1.5	$4 \pm 1.4 \times 10^{-14}$	–
5	6.8 ± 2.9	$6 \pm 1.1 \times 10^{-14}$	30 ± 18
6	8.0 ± 1.9	$2 \pm 1.0 \times 10^{-14}$	–
7	8.9 ± 2.4	$4 \pm 0.9 \times 10^{-15}$	–

5. Results

Ice specimens subjected to falling-head tests, to date, had mean grain diameters of 1.7–8.9 mm (Table 1), with log-normal size distributions (Fig. 4). Grain-size variability tended to increase with increasing mean grain size.

A single value of permeability for a given ice disk generally accounted for variable rates of head decrease under different hydraulic gradients (Fig. 5), indicating that flow over the short periods of the falling-head tests was Darcian. Head-drop data were used to compute multiple permeability values for each test (Fig. 5) using a timescale of differentiation of one-tenth of the test duration. Resultant mean permeability values from tests did not vary systematically with the mean hydraulic gradient (Fig. 6). In falling-head tests immediately repeated at the same head, there was a tendency in some experiments for permeability to be slightly larger in the second test (Figs 5a, 6), although this tendency was not universal. Tests on both fine- and coarse-

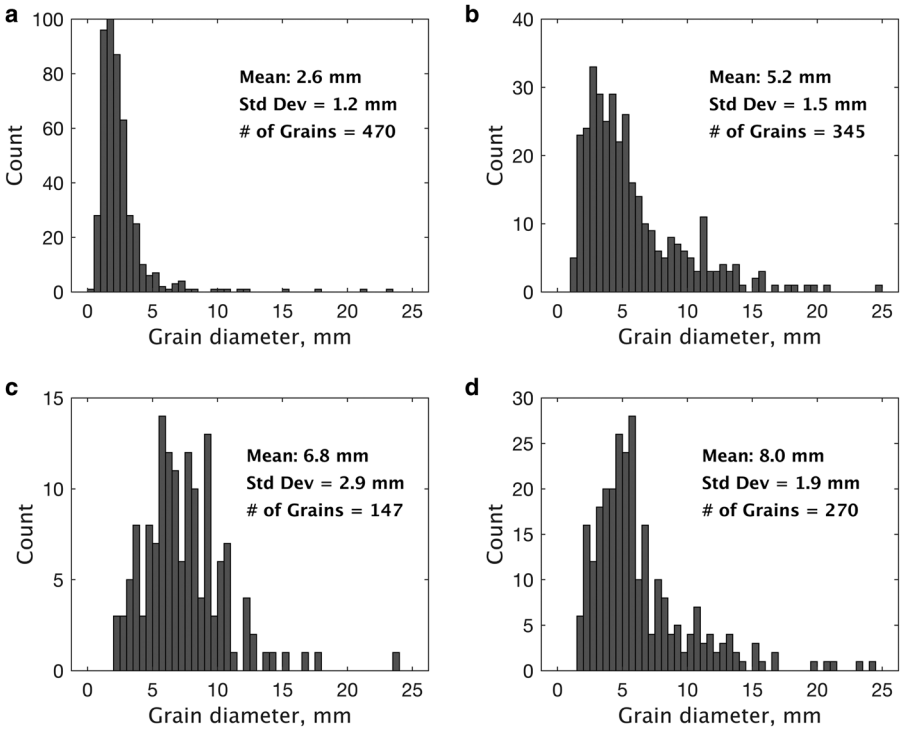

Fig. 4. Grain-size distributions measured from thin sections for ice disks with geometric mean grain sizes of (a) 2.6 mm, (b) 5.2 mm, (c) 6.8 mm and (d) 8.0 mm. Grain-size distributions are log-normal, rather than Gaussian, which is typical for grain-size distributions of glacier ice (Fitzpatrick, 2013).

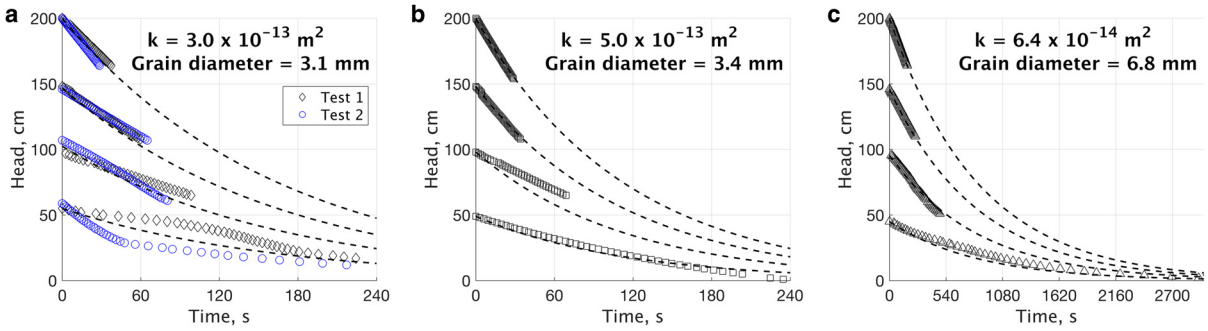

Fig. 5. Head decreases with time for three ice disks for tests begun at different head values. (a) Head-drop data from eight tests on ice with a geometric mean grain diameter of 3.1 mm; two series of tests were conducted in succession at each of the four initial head values. (b) Single-test data from a different ice disk with a comparable mean grain diameter. (c) Single-test data from an ice disk with a mean grain diameter of 6.8 mm. Dashed lines indicate the decrease in head with time for the average permeability value derived for each ice specimen using Eqn (5): (a) 3.0 ± 1.5 x 10^{-13} m^2, (b) 5.0 ± 1.2 x 10^{-13} m^2 and (c) 6.4 ± 1.1 x 10^{-14} m^2. All ice disks were ~50 mm thick, and the ice pressure was 500 kPa (see colors in on-line version).

grained ice yielded permeability values that were independent of hydraulic gradient (Fig. 5b, c).

Although permeability values decreased with increasing grain size (Table 1), the sensitivity to grain size was larger than usually assumed for crystalline rocks with small melt fractions. Over mean grain diameters ranging from 1.7 to 8.9 mm, permeability values decreased from 2×10^{-12} to 4×10^{-15} m^2 (Fig. 7). If the cross-sectional area of veins does not vary with grain size (e.g. Raymond and Harrison, 1975), water content will scale with d^{-2}. In that case, the leading hypothesis is that permeability will also depend on d^{-2} (Eqn 3), assuming homogeneous grain size and structure. The data, however, indicate a more sensitive relationship, with permeability dependent on $d^{-3.4}$ (Fig. 7).

Two experiments conducted, to date, with dye on ice disks with mean grain diameters of 2 and 7 mm provide no evidence that vein diameters were dependent on grain size. Random selection of 24 veins in each ice disk after falling-head tests indicated mean vein radii of 35 ± 20 and 30 ± 18 μm for fine-grained and coarse-grained ice, respectively (Table 1). Variability of radii reflects, in part, the uncertain orientation of veins relative to the plane of observation. Two-tailed *t*-tests applied to the two sets of vein data showed statistically insignificant differences in vein radius between the two ice disks (p-value > 0.40).

Moreover, weighted averages of vein radii, accounting for the quartic dependence of permeability on vein radii (Eqn 3) for the fine and coarse ice disks, were 54 and 43 μm and hence in relatively close agreement.

In contrast, the irregularity of ice grain boundaries tended to increase with increasing grain size. Measurements indicate that grain-boundary tortuosity increased linearly with grain size by ~35% across the fourfold increase in grain size (Fig. 8).

6. Discussion

6.1 Permeability values relative to other studies

Estimates of the permeability of temperate glacier ice vary widely. Raymond and Harrison (1975) estimated the water flux through Blue Glacier. Their maximum flux estimate, predicated on an assumed hydraulic gradient, was commensurate with a permeability

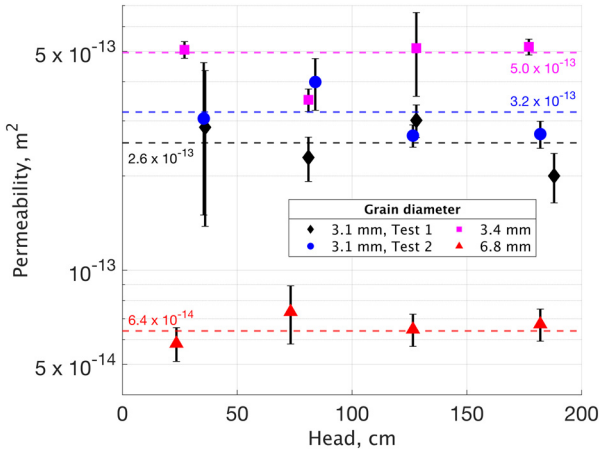

Fig. 6. Permeability as a function of average head magnitude for the test results of Figure 5. Error bars show ±1 SD calculated by considering rates of head decrease over 10 periods of equal duration during each head-drop test. Dashed colored lines indicate mean permeability values for each series of head-drop tests. Note that two of the data sets (blue circles and black diamonds) were collected from the same ice specimen and reflect a first series of tests at different initial head values (black diamonds) followed immediately by a second series of tests (blue circles) (see colors in on-line version).

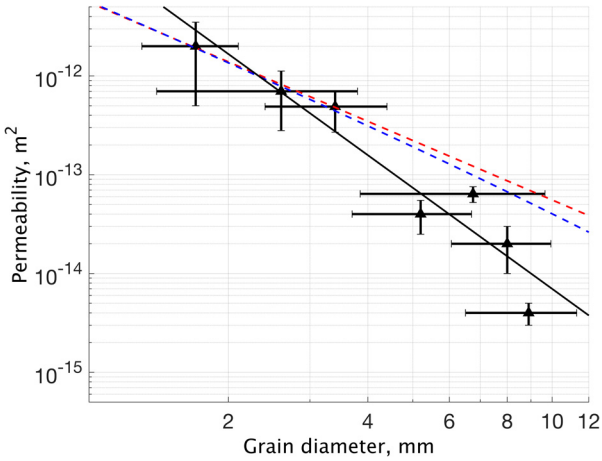

Fig. 7. Permeability as a function of grain diameter from tests on seven ice disks. Error bars show ±1 SD based on multiple permeability tests and the distribution of grain sizes within ice disks. The black line is a best-fit regression of the data, where $k = 1.75 \times 10^{-11}$ ($d^{-3.4}$) with d in millimeters. The dashed red line is a best fit to the data using Eqn (3) and vein radius as a fitting parameter with $r = 45\,\mu m$. The blue dashed line is a best fit to the data using a model adjusted to include vein tortuosity (Eqn 8) with $r = 46\,\mu m$ (see colors in on-line version).

of $8.2 \times 10^{-15}\,m^2$ for bubble-free, fine-grained ice (mean grain size = 2 mm). This value is roughly two orders of magnitude lower than the highest permeability measured in this study for similarly fine-grained ice. However, Raymond and Harrison suggested that the maximum water content of the ice they studied was ~0.1%. The water content of the fine-grained ice studied herein may have been higher.

In the absence of water-content measurements from the initial experiments described herein, we approximate the water content of the ice with an adjusted expression from Frank (1968) that relates volumetric water content to grain size for a specific vein radius:

$$\phi \cong \left[6\pi\sqrt{2}\right]\left[\frac{3\sqrt{3}}{\pi}\right]\frac{r^2}{d^2} = \frac{18\sqrt{6}r^2}{d^2}. \quad (6)$$

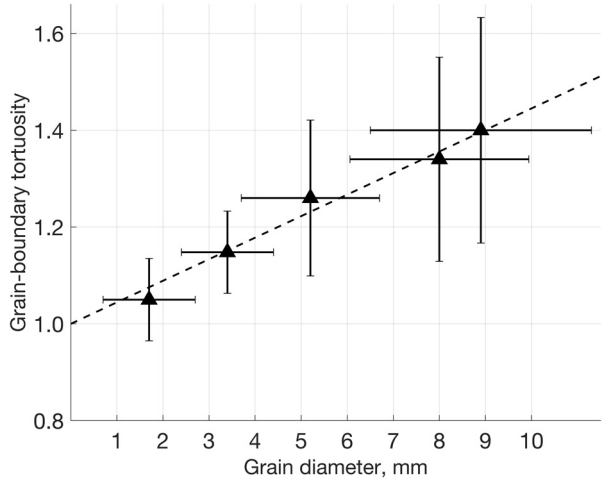

Fig. 8. Mean grain-boundary tortuosity as a function of grain diameter for different ice disks. Error bars show ±1 SD The dashed line is the fitted linear relationship between mean tortuosity, T, and mean grain diameter d, such that $T = 1.0 + 0.048\,d$, with d in millimeters.

The first term in brackets is based on geometrical assumptions of edge length per unit volume for a truncated octahedron. The second bracketed term adjusts Frank's expression that pertained to veins that are circular in cross-section to more realistic veins with triangular cross-sections, retaining the previous definition of r (Fig. 1). Using the area-weighted average, $\bar{r} = \sqrt{\sum r^2/n}$, measured in thin sections from the two ice disks studied with dye ($\bar{r} =$ 41 and 34 μm, respectively), which had mean grain diameters of 2 and 7 mm, Eqn (6) indicates melt fractions of 1.9 and 0.1%, respectively. Note also that if, in contrast, the usual assumption is made that water content does not vary with grain size (Frank, 1968; McKenzie, 1984; Miller and others, 2014), Eqn (6) indicates that the increase in grain size from 2 to 7 mm would require vein radii to increase by a factor of 3.5. Thus, although our vein radii data gathered, to date, are for only these two grain sizes, it is significant that measured mean vein radii for the two grain sizes are nearly equal.

For these estimated water contents of 1.9 and 0.1%, the theory of Nye and Frank (1973), adjusted for veins with triangular cross-sections such that $C = 6.8 \times 10^{-4}$ in Eqn (4), indicates for both grain sizes permeability values that are in good agreement with the data. Equation (4) yields $k = 9.9 \times 10^{-13}\,m^2$ and $k = 3.4 \times 10^{-14}\,m^2$, respectively, for the 2 and 7 mm grain diameters. These values, respectively, are ~60 and ~170% of the best-fit permeability values for these two grain diameters (Fig. 7). Given that potential permeability values may vary through several orders of magnitude, these permeability estimates agree well with our measurements, although these estimates are highly sensitive to the measured average vein radii.

Measured permeability values for the various grain sizes are in the upper part of the range that has sometimes been estimated for temperate ice and other rocks with small melt fractions. Haseloff and others (2019), in their modeling of ice-stream shear margins, considered a range of permeability values, k_w, normalized to water content such that $k_w = k/\phi^2$, consistent with Eqn (4). They thought that possible values for temperate ice were in the range $k_w = 1 \times 10^{-12} - 5 \times 10^{-8}\,m^2$. With the assumption, based on our initial observations, that vein size does not vary with grain size, we use the weighted mean of all vein radii measured ($r =$ 37.5 microns) to compute for the range of grain sizes of Figure 7 the associated range of ϕ (Eqn 6). This exercise yields $k_w = 10^{-9} - 10^{-8}\,m^2$ across the grain sizes of the experiments, which falls in the upper part of the permeability range deemed

reasonable by Haseloff and others (2019). Such large values in their model inhibit strain localization in ice-stream shear margins by promoting small water contents and high ice effective viscosity. Von Bargen and Waff (1986), who studied the permeability of rocks with melt fractions below 5%, calculated permeability values within a factor of 3.0 of the values measured here at comparable fractional melt contents.

The only previous direct laboratory measurement of the permeability of temperate, pure ice yielded values about two to three orders of magnitude lower than those of the present study (Jordan and Stark, 2001). However, the results of these earlier experiments are difficult to interpret in the present context because they were performed under unsaturated conditions. Ice veins not saturated with water will yield values of hydraulic conductivity and apparent permeability that are smaller than for the saturated case by an amount non-linearly proportional to the fraction of vein volume containing air.

6.2 Grain-size dependence

Although permeability models suggest an inverse-squared dependence of permeability on grain size for a given water vein radius (Eqn 3), the data indicate that permeability depends on $d^{-3.4}$ (Fig. 7). For example, if we assume, as indicated by our initial observations, that vein radius does not vary with grain size, then Eqn (4) can be fit to the data using vein radius as a fitting parameter. This exercise, with $B = 1.33$, yields a best fit with $r =$ 45 µm. This value is comparable to those observed, but the d^{-2} dependence results in over-estimated k values for the largest grain sizes (Fig. 7).

A possible explanation is that some other factors may vary systematically with increasing grain size. One such parameter is grain-boundary tortuosity, which our measurements indicate increases linearly with grain size in our ice disks (Fig. 8). If vein tortuosity mimics grain-boundary tortuosity, then Eqn (2) can be adjusted accordingly by scaling the hydraulic gradient with the tortuosity, T, as a function of an ice disk's mean grain size, so the specific discharge is reduced to

$$q = -B\frac{r^4}{d^2}\frac{\rho g}{\mu}\frac{1}{T}\frac{\mathrm{d}h}{\mathrm{d}x} \tag{7}$$

with

$$k = B\frac{r^4}{d^2 T}. \tag{8}$$

Regression of the data of Figure 8 indicates that $T = 1 + 0.048d$, with d in millimeters. Fitting Eqn (8) to the data, with this relation for T and again with vein radius as a fitting parameter, yields a vein radius comparable to that observed, $r = 46$ mm, but with only slightly increased sensitivity of k values to grain size and, as before, over-estimation of k for the largest grain sizes (Fig. 7).

Past work points to two other hypotheses for the heightened sensitivity of k values to grain size. Raymond and Harrison (1975) suggested that air bubbles block veins in coarse-grained ice more than in fine-grained ice, to the extent that water flux through coarse-bubbly ice may be as low as 6% of that for clear ice. Coarse ice has fewer crystal boundaries per unit ice volume, causing air bubbles to concentrate along the more limited edge length and resulting in a higher probability of obstruction (Raymond and Harrison, 1975). Although the method of ice preparation used for these experiments eliminates most air from the ice, the ice is not perfectly transparent and small bubbles (<300 µm) are present. Thus, this hypothesis cannot be rejected. Another possibility is that increasing grain-boundary tortuosity with the increasing grain size reduces vein continuity. Mader's (1992) detailed observations of vein geometry revealed many pinched-off veins, and she considered them to be a viable mechanism for limiting permeability. A reasonable hypothesis, therefore, is that as grain boundaries become more irregular, the probability of truncated veins increases, reducing ice permeability.

A final hypothesis is that water content was smaller in the coarse-grained ice than if vein radii were constant with grain size, remembering that the latter assumption gives rise to the dependence of k on d^{-2}. More specifically, vein radii would need to have been systematically smaller in the coarse-grained ice to result in the dependence on $d^{-3.4}$. We cannot reject this hypothesis without water-content data or more extensive vein-size data.

The increase in permeability with d^2 indicated by Eqn (4) is predicated on considering a geometrically-based relationship, such as Eqn (6), and assuming that water content does not vary with grain size – a requirement for a closed system. This assumption, which has been made for glacier ice (Schoof and Hewitt, 2016; Haseloff and others, 2019) and is routine in the rock physics literature (e.g. Miller and others, 2014), requires that vein radii increase linearly with grain size. In contrast, in these experiments, in which heat and water can flow across the ice-disk boundaries, our initial observations suggest, as noted, that vein radii do not vary with grain size. Similarly, in the open system of a temperate glacier, Raymond and Harrison (1975) found, in the only such study to date, no difference in vein size in ice with two different mean grain sizes, 2 and 7 mm, values within the range considered here. From this they inferred, together with later authors (e.g. Lliboutry, 1996; Hooke, 2020) and consistent with our results, that coarse-grained ice, owing to its lower density of veins, is less permeable than fine-grained ice.

6.3 Limitations

Despite initial data from the device that are internally consistent and in reasonable agreement with estimates of some theoretical studies, the new apparatus does not allow a complete simulation of interstitial water flow in a temperate glacier. Most importantly, the permeability measured in these experiments cannot be viewed as being adjusted to the applied ice pressure. Our method relies on inducing transient water flow through ice usually over time scales of seconds to several days, whereas the timescale for vein shrinkage by viscous creep (i.e. viscous compaction) of ice under pressure (e.g. Schoof and Hewitt, 2016) is thought to be much longer. Viscous compaction cannot be measured in the experiments because, although thinning of the ice disk with time is measured, most of the thinning is due to melting at the edges of the ice disk, which obscures any component of thinning from compaction. Raymond and Harrison (1975) observed no significant variation in water vein radius over a sixfold increase in ice depth up to 60 m, providing no evidence of viscous compaction. Nevertheless, we cannot rule out that steady water flow over much longer time scales might obey a non-Darcian discharge–head relationship, as suggested by Lliboutry (1996). Importantly, the pressure applied to the ice disks is, nevertheless, essential for the success of the experiments. The resultant pressure in the water film at the ice disk's lateral edges prevents preferential flow of through-going water there that would otherwise corrupt the permeability measurement.

Minimum head gradients that can be applied with the device are likely larger than in most temperate ice of glaciers. The minimum head gradient applied herein was ~0.1. This value likely exceeds potential gradients in glacier ice except perhaps where

steep velocity gradients and associated gradients of viscous heat dissipation persist.

Another difference from conditions in a glacier is that the ice, except for some minor volumetric strain, undergoes no deformation. Deformation would affect water-vein network geometry over long time scales by inducing recrystallization processes. Also, lack of shear deformation and associated heat dissipation exclude from experiments the primary source of heat and internal melting in glacier ice. The only source of heat available for internal melting in the experiments is, instead, the conductive heat flux into the ice specimen resulting from the slight depression of the PMT within the ice disk relative to its boundaries (e.g. Nye, 1991b). This minimization of internal melting is, indeed, necessary for the experiment to succeed. Internal melting that is too rapid would cause internal pore pressure too high to allow externally introduced water to flow through the disk under the applied head. Thus, as in most laboratory experiments in the geosciences, the goal here is not simulation, which is almost never possible owing to timescale and boundary problems, but manipulation – in this case to create conditions that allow ice permeability to be measured with a simple approach.

6.4 Future work

Our most pressing priority is to study the dependence of ice permeability on water content by varying it systematically and measuring it using the calorimetric method described herein and used previously (Duval, 1977; Adams and others, 2021). This dependence for both ice and other rocks with a melt phase is viewed as more uncertain than the dependence of permeability on ice grain size (e.g. Miller and others, 2014). The simplest hypothesis (Eqn 4) can be tested by conducting experiments on ice disks with the same grain size but made with different salinities. Bulk ionic concentrations and the NaCl-phase diagram (Weeks and Ackley, 1982) would allow water content to be varied. In addition, different sets of these experiments would need to be conducted for different grain sizes to fully evaluate the power-law dependence of Eqn (4), which is predicated, as previously noted, on the radii of water veins increasing linearly with increasing grain diameter. As noted, our initial observations of veins and those of Raymond and Harrison (1975) do not support this idea. Testing of Eqn (4) – or proposed variations of it with different water-content exponents – will therefore require comprehensive measurements of vein radii in ice disks of different grain sizes.

Extending these measurements to glacier ice is also a high priority, with the goal of studying the effect of ice foliation on the magnitude and anisotropy of ice permeability. The foliation that results from variations in crystal size and shape, debris content, and air-bubble concentration and shape (Hudleston, 2015; Hooke, 2020) should affect the geometry of water-vein networks and their susceptibility to plugging by air bubbles (e.g. Raymond and Harrison, 1975; Lliboutry, 1996). Knowledge of permeability anisotropy is required to define the full range of grain-scale permeability possible in glacier ice and may be particularly important for modeling ice-stream shear margins. As noted, water routed to the bed from shear margins likely plays a central role in controlling the effective stress at the bed and basal-slip distribution (Suckale and others, 2014; Perol and Rice, 2015; Perol and others, 2015; Meyer and others, 2018; Haseloff and others, 2019). Vertical or steeply-dipping longitudinal foliation that is expected in shear margins may significantly enhance vertical permeability and hence flow of water from where it is generated in shear margins downward to the bed. In addition to affecting basal slip, this enhanced downward flow of water would decrease the water content of shear-margin ice (Haseloff and others, 2019), increasing its effective viscosity (Duval, 1977; Adams and others, 2021). Although extracting cores from the deep, temperate ice of shear margins is currently not possible, collecting shallow cores from an accessible temperate glacier would be inexpensive and straightforward. Disks cut from 140 mm-diameter cores with various styles and orientations of foliation would fit the permeameter. Measurements of permeability anisotropy would provide empirical grounding that is currently lacking for modeling ice-stream margins and other parts of glaciers as two-phase flows.

7. Conclusions

A new permeameter, operated in a cold room, allows the permeability of temperate, polycrystalline ice to be measured. An ice disk is kept under pressure and at the pressure-melting temperature while chilled water transiently flows through the disk under a potential gradient that is allowed to decrease with time. The rate of head decrease provides the permeability, and the rate of passage of a freezing front through the ice measured with thermistors can provide the ice water content immediately following the permeability measurement. Chilled water with fluorescein dye introduced to ice disks allows vein networks and the cross-sectional areas of veins to be studied in thin sections after experiments.

Results of initial experiments with lab-made ice, in which water content was not measured, indicate that under the short time scales of the experiments (seconds to hours) flow is Darcian. Over mean grain diameters of $d = 1.7$–8.9 mm, permeability decreases from 2×10^{-12} to 4×10^{-15} m^2. Average area-weighted radii of randomly selected veins, 41 and 34 μm, respectively, in fine-grained (2 mm) and coarse-grained (7 mm) ice, are not significantly different, in agreement with the field observations of Raymond and Harrison (1975). These radii, if included in the theory of Nye and Frank (1973) adjusted to account for vein cross-sections modeled as triangles, yield permeability values within less than a factor of 2 of best-fit values based on regression of the data. Assuming vein size is indeed independent of grain size, permeability scales with $d^{-3.4}$ rather than, as is usually assumed, d^{-2}. Increases in potential clogging effects of air bubbles in coarse-grained ice (Raymond and Harrison, 1975), observed increases in grain-boundary tortuosity with increasing grain size that truncate water veins (Mader, 1992), or vein sizes that decrease sufficiently with increasing grain size may be responsible for this higher-than-expected sensitivity.

Despite some clear limitations of the new device – for example, permeability measurements over durations that are likely too short to allow water flow to adjust to the ice pressure and applied hydraulic gradients that are likely larger than those of glacier ice – future work with it can help establish the relationship between permeability and water content necessary to model temperate parts of glaciers as two-phase flows. Moreover, cores from glaciers would allow the effect of ice-foliation style and orientation on permeability to be evaluated, which may be particularly germane to permeability anisotropy in ice-stream shear margins where strong longitudinal foliation is expected.

Data. The data presented in this paper will be made available at the US Antarctic Data Center repository (https://www.usap-dc.org/) prior to final publication.

Acknowledgements. This research was supported by the US National Science Foundation (NSFGEO-NERC-1643120). We thank J. Misra and T. Herrman of the DOE Ames Laboratory for help designing and constructing the permeameter. Two anonymous reviewers and associate chief editor, Ralf Greve, provided helpful comments.

Author contributions. NRI designed and supervised the construction of the permeameter. JRF executed the experiments, analyzed the ice and analyzed the data, with contributions from NRI. Both authors helped design the experiments and write the paper.

References

Adams CJC, Iverson NR, Helanow C, Zoet LK and Bate CE (2021) Softening of temperate ice by interstitial water. *Frontiers in Earth Science* **9**, 702761. doi: 10.3389/feart.2021.702761

Alley KA, Scambos TA, Alley RB and Holschuh N (2019) Troughs developed in ice-stream shear margins precondition ice shelves for ocean-driven break-up. *Science Advances* **5**(10), eaax2215. doi: 10.1126/sciadv.aax2215

Asaithambi NS (1988) On a variable time-step method for the one-dimensional Stefan problem. *Computer Methods in Applied Mechanics and Engineering* **71**(1), 1–13. doi: 10.1016/0045-7825(88)90092-8

Aschwanden A and Blatter H (2009) Mathematical modeling and numerical simulation of polythermal glaciers. *Journal of Geophysical Research* **114**(F1). doi: 10.1029/2008jf001028

Aschwanden A, Bueler E, Khroulev C and Blatter H (2012) An enthalpy formulation for glaciers and ice sheets. *Journal of Glaciology* **58**(209), 441–457. doi: 10.3189/2012JoG11J088

Dani KGS, Mader HM, Wolff EW and Wadham JL (2012) Modelling the liquid-water vein system within polar ice sheets as a potential microbial habitat. *Earth and Planetary Science Letters* **333-334**, 238–249. doi: 10.1016/j.epsl.2012.04.009

Durand G (2004) *Microstructure, recristallisation et déformation des glaces polaires de la carotte EPICA, Dôme Concordia, Antarctique* (Doctoral dissertation). Université Joseph-Fourier, Grenoble, France. Available at https://tel.archives-ouvertes.fr/tel-00701364/file/These-Durand-2004-1.pdf.

Duval P (1976) *Fluage et recristallisation des glaces polycristallines* (Doctoral dissertation). Université Scientifique et Médicale de Grenoble, Saint-Martin-d'Hères, France.

Duval P (1977) The role of the water content on the creep rate of polycrystalline ice. *International Association of Hydrological Sciences Publication* **118**, 29–33.

Duval P and Le Gac H (1980) Does the permanent creep-rate of polycrystalline ice increase with crystal size? *Journal of Glaciology* **25**(91), 151–158. doi: 10.3189/S0022143000001036425(91

Eicken H, Krouse HR, Kadko D and Perovich DK (2002) Tracer studies of pathways and rates of meltwater transport through Arctic summer sea ice. *Journal of Geophysical Research: Oceans* **107**(C10), 8046. doi: 10.1029/2000JC000583

Fitzpatrick JJ (2013) Digital-image processing and image analysis of glacier ice. In Automated data processing and computations. (USGS Techniques and Methods 7) US Geological Survey, Reston, VA. doi: 10.3133/tm7D1

Fowler AC (1984) On the transport of moisture in polythermal glaciers. *Geophysical and Astrophysical Fluid Dynamics* **28**(2), 99–140. doi: 10.1080/03091928408222846

Frank FC (1968) Two-component flow model for convection in the earth's upper mantle. *Nature* **220**(5165), 350–352. doi: 10.1038/220350a0

Freeze RA and Cherry JA (1979) *Groundwater*. Englewood Cliffs, NJ: Prentice-Hall

Greve R (1997) A continuum-mechanical formulation for shallow polythermal ice sheets. *Philosophical Transactions of the Royal Society of London A* **355** (1726), 921–974. doi: 10.1098/rsta.1997.0050

Haseloff M, Hewitt IJ and Katz RF (2019) Englacial pore water localizes shear in temperate ice stream margins. *Journal of Geophysical Research: Earth Surface* **124**(11), 2521–2541. doi: 10.1029/2019F005399

Haseloff M, Schoof C and Gagliardini O (2015) A boundary layer model for ice stream margins. *Journal of Fluid Mechanics* **781**, 353–387. doi: 10.1017/jfm.2015.503

Hewitt IJ and Schoof C (2017) Models for polythermal ice sheets and glaciers. *Cryosphere* **11**(1), 541–551. doi: 10.5194/tc-11-541-2017

Hooke RL (2020) *Principles of Glacier Mechanics*, 3rd Edn. Cambridge: Cambridge University Press. doi: 10.1002/vzj2.20073

Hudleston PJ (2015) Structures and fabrics in glacial ice: A review. *Journal of Structural Geology* **81**, 1–27. doi: 10.1016/j.jsg.2015.09.003

Hunter P, Meyer C, Minchew B, Haseloff M and Rempel A (2021) Thermal controls on ice stream shear margins. *Journal of Glaciology* **67**(263), 435–439. doi: 10.1017/ jog.2020.118

Hutter K (1982) A mathematical model of polythermal glaciers and ice sheets. *Geophysical and Astrophysical Fluid Dynamics* **21**(3-4), 201–224. doi: 10.1080/03091928208209013

IMBIE Team (2020) Mass balance of the Greenland Ice Sheet from 1992 to 2018. *Nature* **579**(7798), 233–239. doi: 10.1038/s41586-019-1855-2

Iverson NR and Petersen BB (2011) A new laboratory device for study of subglacial processes: first results on ice–bed separation during sliding. *Journal of Glaciology* **57**(206), 1135–1146. doi: 10.3189/002214311798843458

Jordan RE and Stark JA (2001) Capillary tension in rotting ice layers (No. ERDC/CRREL-TR-01–13) Engineer Research and Development Center, Hanover, NH, Cold Regions Research and Engineering Lab. Available at https://apps.dtic.mil/sti/pdfs/ADA399589.pdf.

Kamb B (2001) Basal zone of the West Antarctic ice streams and its role in lubrication of their rapid motion. *The West Antarctic Ice Sheet: Behavior and Environment* **77**, 157–199. doi: 10.1029/ar077p0157.

Kizito F and 6 others (2008) Frequency, electrical conductivity and temperature analysis of low-cost moisture sensor. *Journal of Hydrology*, **352**(3–4), 367–378. doi: 10.1016/j.jhydrol.2008.01.021

Kyrke-Smith TM, Katz RF and Fowler AC (2014) Subglacial hydrology and the formation of ice streams. *Proceeding of the Royal Society A* **470**(2161), 20130494. doi: 10.1098/rspa.2013.0494

Kyrke-Smith TM, Katz RF and Fowler AC (2015) Subglacial hydrology as a control on emergence, scale and spacing of ice streams. *Journal of Geophysical Research: Earth Surface* **120**(8), 1501–1514. doi: 10.1002/2015JF003505

Lambe TW and Whitman RV (1969) *Soil Mechanics*. New York: John Wiley & Sons, Inc

Lekner J (2007) Viscous flow through pipes of various cross-sections. *European Journal of Physics* **28**(3), 521–527. doi: 10.1088/0143-0807/28/3/014

Lliboutry L (1971) Permeability, brine content and temperature of temperate ice. *Journal of Glaciology* **10**(58), 15–29. doi: 10.3189/s002214300001296x

Lliboutry L (1996) Temperate ice permeability, stability of water veins and percolation of internal meltwater. *Journal of Glaciology* **42**(141), 201–211. doi: 10.1017/s0022143000004068

Mader HM (1992) Observations of the water-vein system in polycrystalline ice. *Journal of Glaciology* **38**(130), 333–337. doi: 10.3189/s0022143000002227

Mader HM, Pettitt ME, Wadham JL, Wolff EW and Parkes RJ (2006) Subsurface ice as a microbial habitat. *Geology* **34**(3), 169–172. doi: 10.1130/g22096.1

McKenzie D (1984) The generation and compaction of partially molten rock. *Journal of Petrology* **25**(3), 713–765. doi: 10.1093/petrology/25.3.713

Meyer CR and Minchew BM (2018) Temperate ice in the shear margins of the Antarctic Ice Sheet: controlling processes and preliminary locations. *Earth and Planetary Science Letters* **498**, 17–26. doi: org/10.1016/j.epsl.2018.06.028

Meyer CR, Yehya A, Minchew B and Rice JR (2018) A model for the downstream evolution of temperate ice and subglacial hydrology along ice stream shear margins. *Journal of Geophysical Research: Earth Surface* **123**(8), 1682–1698. doi: 10.1029/2018JF004669

Miller KJ, Zhu WL, Montési LGJ and Gaetani GA (2014) Experimental quantification of permeability of partially molten mantle rock. *Earth and Planetary Science Letters* **388**, 273–282. doi: 10.1016/j.epsl.2013.12.003

Minchew B, Meyer CR, Robel AA, Gudmundsson GH and Simons M (2018) Processes controlling the downstream evolution of ice rheology in glacier shear margins: case study on Rutford Ice Stream, West Antarctica. *Journal of Glaciology* **64**(246), 583–594. doi: 10.1017/jog.2018.47

Nye JF (1989) The geometry of water veins and polycrystalline ice. *Journal of Glaciology* **35**(119), 17–22. doi: 10.3189/002214389793701437

Nye JF (1991a) Thermal behavior of glacier and laboratory ice. *Journal of Glaciology* **37**(127), 401–413. doi: 10.3189/s0022143000005839

Nye JF (1991b) The rotting of temperate ice. *Journal of Crystal Growth* **113**(3–4), 465–476. doi: 10.1016/0022-0248(91)90081-f

Nye JF and Frank FC (1973) Hydrology of the intergranular veins in a temperate glacier. *International Association of Scientific Hydrology* **95**, 157–161.

Nye JF and Mae S (1972) The effect of non-hydrostatic stress on intergranular water veins and lenses in ice. *Journal of Glaciology* **11**(61), 81–101. doi: 10.1017/s0022143000022528

Perol T and Rice JR (2015) Shear heating and weakening of the margins of West Antarctic ice streams. *Geophysical Research Letters* **42**(9), 3406–3413. doi: 10.1002/2015GL063638

Perol T, Rice JR, Platt JD and Suckale J (2015) Subglacial hydrology and ice stream margin locations. *Journal of Geophysical Research: Earth Surface* **120** (7), 1352–1368. doi: 10.1002/2015JF003542

Platt JD, Perol T, Suckale J and Rice JR (2016) Determining conditions that allow a shear margin to coincide with a Röthlisberger channel. *Journal of Geophysical Research: Earth Surface* **121**(7), 1273–1294. doi: 10.1002/2015JF003707

Price PB (2000) A habitat for psychrophiles in deep Antarctic ice. *Proceedings of the National Academy of Sciences* **97**(3), 1247–1251. doi: 10.1073/pnas.97.3.1247

Raymond CF and Harrison WD (1975) Some observations on the behavior of the liquid and gas phases in temperate glacier ice. *Journal of Glaciology* **14** (71), 213–233. doi: 10.3189/s0022143000021717

Rignot E and 5 others (2019) Four decades of Antarctic Ice Sheet mass balance from 1979-2017. *Proceedings of the National Academy of Sciences* **116**(4), 1095–1103. doi: 10.1073/pnas.1812883116

Robinson DA, Jones SB, Wraith JM, Or D and Freidman SP (2003) A review of advances in dielectric and electrical conductivity measurement in soils using time domain reflectometry. *Vadose Zone Journal* **2**(4), 444–475. doi: 10.2136/vzj2003.0444

Schoof C and Hewitt IJ (2016) A model for polythermal ice incorporating gravity-driven moisture transport. *Journal of Fluid Mechanics* **797**, 504–535. doi: 10.1017/jfm.2016251

Suckale J, Platt JD, Perol T and Rice JR (2014) Deformation induced melting in the margins of the West Antarctic ice streams. *Journal of Geophysical Research: Earth Surface* **119**(5), 1004–1025. doi: 10.1002/2013JF003008

Thompson AC, Iverson NR and Zoet LK (2020) Controls on subglacial rock friction: experiments with debris in temperate ice. *Journal of Geophysical Research: Earth Surface* **125**(10). doi: 10.1029/2020JF005718

Todd DK (1961) *Groundwater Hydrology*. London: Chapman & Hall. doi: 10.1002/qj.49708737126

von Bargen N and Waff HS (1986) Permeabilities, interfacial areas and curvatures of partially molten systems: results of numerical computations of equilibrium microstructures. *Journal of Geophysical Research* **91**(B9), 9261–9276. doi: 10.1029/JB091iB09p09261

Weeks WF and Ackley SF (1982) The growth, structure, and properties of sea ice (No. ADA123762). Engineer Research and Development Center, Hanover, NH, Cold Regions Research and Engineering Lab. Available at https://apps.dtic.mil/sti/pdfs/ADA123762.pdf

West LJ, Ripin DM, Murray T, Mader HM and Hubbard B (2007) Dielectric permittivity measurements on ice cores: implications for interpretations of radar to yield glacial unfrozen water content. *Journal of Environmental and Engineering Geophysics* **12**(1), 37–45. doi: 10.2113/jeeg12.1.37

Zhou X, Zhou J, Kinzelbach W and Stauffer F (2014) Simultaneous measurement of unfrozen water content and ice content in frozen soil using gamma ray attenuation and TDR. *Water Resources Research* **50**(12), 9630–9655. doi: 10.1002/2014WR015640

Zhu W and Hirth G (2003) A network model for permeability in partially molten rocks. *Earth and Planetary Science Letters* **212**(3-4), 407–416. doi: 10.1016/s0012-821x(03)00264-4

Zoet LK and Iverson NR (2020) A slip law for glaciers on deformable beds. *Science (New York, N.Y.)* **368**(6486), 76–78. doi: 10.1126/science. aaz1183